IRIS AperTO

UNIVERSITÀ DEGLI STUDI DI TORINO

AperTO - Archivio Istituzionale Open Access dell'Università di Torino

**Insights into the Rb-Mg-N-H System: An Ordered Mixed Amide/Imide Phase and a Disordered Amide/Hydride Solid Solution**

**This is the author's manuscript**

*Original Citation:*

*Availability:*

This version is available http://hdl.handle.net/2318/1687750 since 2019-01-23T14:27:04Z

*Published version:*

DOI:10.1021/acs.inorgchem.7b03232

*Terms of use:*

Open Access

Anyone can freely access the full text of works made available as "Open Access". Works made available under a Creative Commons license can be used according to the terms and conditions of said license. Use of all other works requires consent of the right holder (author or publisher) if not exempted from copyright protection by the applicable law.

(Article begins on next page)

18 April 2024

# *New insights into the Rb-Mg-N-H system: an ordered mixed amide/imide phase and a disordered amide/hydride solid solution*

*Antonio Santoru,*[,a] Claudio Pistidda,[a] Matteo Brighi,[b] Michele R. Chierotti,[c] Michael Heere,[d] Fahim Karimi,[a] Hujun Cao,[a] Giovanni Capurso,[a] Anna-Lisa Chaudhary,[a] Gökhan Gizer,[a] Sebastiano Garroni,[e,f] Magnus H. Sørby,[d] Bjørn C. Hauback,[d] Radovan Černý,[b] Thomas Klassen,[a] Martin Dornheim[a]*

a) Nanotechnology Department, Helmholtz-Zentrum Geesthacht Max-Planck Straße 1, 21502, Geesthacht, Germany

b) Laboratory of Crystallography, Department of Quantum Matter Physics, University of Geneva, Quai Ernest-Ansermet 24, Ch-1211, Geneva, Switzerland

c) Department of Chemistry and NIS centre, University of Torino, V. Giuria 7, 10125, Torino, Italy

d) Physics Department, Institute for Energy Technology (IFE), P.O. Box 40, NO-2027 Kjeller, Norway

e) International Research Centre in Critical Raw Materials-ICCRAM, University of Burgos, Plaza Misael Banuelos s/n, 09001 Burgos, Spain

f) Advanced Materials, Nuclear Technology and Applied Bio/Nanotechnology. Consolidated Research Unit UIC-154. Castilla y Leon. Spain. University of Burgos. Hospital del Rey s/n, 09001 Burgos, Spain

To whom correspondence should be addressed. E-mail: antonio.santoru@hzg.de

KEYWORDS: metal amides, metal hydrides, solid solution, structure solution, synchrotron X-ray diffraction, powder neutron diffraction, solid state NMR

ABSTRACT

The crystal structure of a mixed amide-imide phase, $RbMgND_2ND$, has been solved in the orthorhombic space group *Pnma* (*a* = 9.55256(31), *b* = 3.70772(11) and *c* = 10.08308(32) Å). A new metal amide-hydride solid solution, $Rb(NH_2)_xH_{(1-x)}$, has been isolated and characterized in the entire compositional range. The profound analogies, as well as the subtle differences, with the crystal chemistry of $KMgND_2ND$ and $K(NH_2)_xH_{(1-x)}$ are thoroughly discussed. This approach suggests that the comparable performances obtained using K- and Rb-based additives for the Li-Mg-N-H hydrogen storage system are likely to depend on the structural similarities of possible reaction products and intermediates.

INTRODUCTION

The discovery of alkali metal amides dates back to the 19$^{th}$ century: Davy, Thenárd and Gay-Lussac discovered the amides of potassium and sodium by studying the effect of these alkali metals on ammonia.[1-3] The possibility of forming Li-N-H phases from $Li_3N$ and $H_2$ was first reported in the 1910 by Dafert and Miklauz.[4] However these results didn't receive remarkable attention from the scientific community until 2002, when Chen and co-workers reported the promising role of metal amides - hydrides composites as hydrogen storage materials.[5] An intense research activity stem from this seminal work, and still continues today, exploring systematically the possible combinations of metal amides with metal hydrides, in order to find optimal hydrogen stores and determine their fundamental properties.[6] With a reaction enthalpy of about 40 kJ/mol $H_2$, the

$Mg(NH_2)_2$+2LiH composite is regarded as one of the most promising systems derived from this research field.[7] However, for its combination with proton-exchange-membrane fuel cells (PEM-FC) in light duty vehicles, additional efforts are needed to improve its reaction kinetics at low temperatures. Low operating temperatures are also necessary to prevent the release of ammonia, thus limiting the risk of poisoning the fuel cell. The addition of potassium based inorganic salts (e.g. potassium hydride, hydroxide and halides) has led to improved sorption properties, including lower ammonia release during desorption and hydrogen reabsorption to 75% of the original hydrogen capacity in only 12 min at 143ºC and 30 bar of $H_2$.[8-18] Recently, the total or partial replacement of potassium with rubidium was also proven to be a successful step to further improve the performance of the overall system.[19-23] Furthermore, it was reported that the enhanced sorption properties account for an alteration of its thermodynamic stability and kinetic behavior, caused by the addition of small amounts of RbH.[20] Despite the fact that possible reaction pathways were proposed, the key reaction product formed from the additive, $RbMgNH_2NH$, was still unknown from the structural point of view. In the present work, we were able to synthesize this novel compound and to solve its crystal structure. Additionally, we identified and characterized a new intermediate of the Rb-N-H system, which is likely to be identified in future Rb-containing amide/hydride systems. In the final stage, an overview of the structural analogies between the potassium and the rubidium case is presented.

## EXPERIMENTAL SECTION

$Mg(NH_2)_2$ was synthesized by ball milling of $MgH_2$ (Rockwood Lithium, 99.8 % of Mg) under 7 bar of $NH_3$ at 400 RPM during 19 h. RbH was obtained *via* ball milling of Rb (Alfa Aesar, 99.75 %) under 50 bar of $H_2$ at 500 RPM for 13 h. $Rb_2Mg(NH_2)_4$ was synthesized by mechanochemical treatment of rubidium (Alfa Aesar, 99.75 %) and magnesium (Aldrich, 99 %)

with a molar ratio of 2:1 under 7 bar of $NH_3$ for 34 h. The sample was then transferred to a stainless steel reactor and heated up to 270 °C for 48 h under 7 bar of $NH_3$. $Rb_2Mg(ND_2)_4$ for neutron diffraction experiments was synthesized by heating Rb and Mg (molar ratio 2:1) under 5 bar of deuterated ammonia ($ND_3$, Aldrich, isotopic purity: 99 atom % D) for more than 48 h at 300 °C in a stainless steel reactor. $MgD_2$ was prepared by annealing of previously desorbed $MgH_2$ under ~ 120 bar of deuterium ($D_2$, Air Liquid, 99.8 mol%) at 400 °C for 24 h. The compounds were subsequently mixed in the desired ratio using an agate mortar and pestle. The mixture was then desorbed under dynamic vacuum at 260 °C for 1 h.

$RbNH_2$ was prepared by heating rubidium under 7 bar of ammonia up to 250 °C for about 13 h. RbH was prepared by ball milling of Rb under 50 bar of $H_2$ for 23 h at 600 RPM, followed by 17 h at 400 RPM. All compositions were prepared by mixing the corresponding amounts of $RbNH_2$ and RbH with an agate mortar and pestle. The annealed samples were prepared by heating the hand-ground mixtures up to 200 °C for 4 h under argon atmosphere.

All milling procedures under reactive gases were performed using a high pressure vial (Evico Magnetics, Germany) and a Pulverisette 6 planetary mill (Fritsch, Germany).

All samples were handled in argon-filled glove-boxes (mBraun, Germany) with oxygen and water levels lower than 5 ppm, in order to avoid their oxidation and/or hydrolysis.

*Ex situ* X-ray powder diffraction (XPD) experiments were performed on a D8 Discover (Bruker, Germany) in Bragg-Brentano geometry equipped with a copper source ($\lambda$ = 1.54184 Å) and 2D VANTEC detector. The sample was placed in a flat commercial sample holder, sealed from the top with a dome of poly(methyl methacrylate) (PMMA) that prevents its exposure to air.

The *ex-situ* synchrotron radiation X-ray powder diffraction (SR-XPD) pattern for structure solution was collected at the Swiss Norwegian Beamlines (SNBL) of the European Synchrotron Radiation Facility (ESRF, Grenoble, France). Data were recorded on a Dectris Pilatus 2M detector at a wavelength of 0.8212 Å. 2D images were integrated and treated with the locally written program Bubble.[24]

Neutron powder diffraction (NPD) was performed at the PUS instrument of the JEEP II reactor (IFE, Norway).[25] A Ge(111) monochromator with 90° take-off angle provided neutrons with wavelength of 1.55357 Å. The data were recorded with two detector banks, each with 7 vertically stacked position-sensitive detectors covering 20° in 2θ. The total angular range is 2θ = 10°-130°, and angular step size Δ2θ = 0.05°. The sample was contained in a vanadium container with 6 mm inner diameter.

Structure solution was carried out with the FOX program.[26] Rietveld refinement[27, 28] of the XPD data was performed with the software MAUD (Material Analysis Using Diffraction).[29] Rietveld refinement of the NPD data was performed with the software GSAS (General Structure Analysis System)[30] implementing the graphical user interface EXPGUI.[31] The software VESTA[32] was used for building the graphical models of the crystal structures, standardization of crystal data, as well as calculating the interatomic distances reported in Table 2 and S2.

The *in situ* XPD experiments were performed at the High Energy Material Science (HEMS) diffraction beamline (P07) of Petra III (Hamburg, Germany). The beamline provides a monochromatic X-ray beam (λ = 0.14235 Å). The diffraction images were collected with a Perkin Elmer XRD 1621 Flat Panel, using an exposure time of 15 s per scan. The powdered samples were packed inside sapphire capillaries with 0.6 mm inner diameter, which were mounted on in-house

developed sample holders allowing for well controlled temperature and pressure conditions. All measurements were performed under 1 bar of argon, heating up from room temperature (RT) to 270 °C with an heating rate of 10 °C/min, maintaining isothermal conditions at 270 °C (5 min for the pristine $RbNH_2$ and RbH, 10 min for their mixtures) and then cooling down to RT at 10 °C/min.

Attenuated total reflection infrared spectroscopy (ATR-IR) measurements were performed using a Bruker Alpha-Platinum infrared spectrometer and a diamond crystal. The spectrum was obtained at RT in the range of 4000-400 $cm^{-1}$ and at a resolution of 2 $cm^{-1}$, with 32 scans averaged for each spectrum and the background. The samples were measured without any dilution. The spectrometer was situated inside an Ar-filled atmosphere controlled glove box.

Solid-state NMR experiments were run on a Bruker AVANCE II 400 instrument operating at 400.23 MHz for $^1H$ and equipped with a 2.5 mm probe. Rotors were packed inside a glove-box to prevent sample decomposition. The $^1H$ MAS spectra were acquired at the spinning speed of 32 kHz with the DEPTH sequence ($\pi/2$-$\pi$-$\pi$) for the suppression of the probe background signal ($^1H$ 90° = 2.5 μs; scans = 16; relaxation delays equal to 1.27-5*$T_1$). Relaxation measurements were performed with a saturation recovery pulse sequence. 2D $^1H$ DQ MAS experiments were performed at 32 kHz with the back-to-back (BABA) recoupling pulse sequence with excitation times of one rotor period ($^1H$ 90° = 2.5 μs; 32 scans; $t_1$ increments = 46; relaxation delays equal to 1.27-5*$T_1$). $^1H$ scale was calibrated with adamantane ($^1H$ signal at 1.87 ppm) as external standard.

## RESULTS AND DISCUSSION

### Synthesis of $RbMgNH_2NH$

It was previously reported that a 1:1 mixture of $Mg(NH_2)_2$ and RbH forms $RbMgNH_2NH$ while releasing an equivalent mole of $H_2$ when heated to 250 °C. Therefore the following reaction (1) was proposed:[20]

1) $Mg(NH_2)_2 + RbH \rightarrow RbMgNH_2NH + H_2$

Our diffraction experiment (Fig. 1-a) shows no Bragg reflections of the starting materials in the product obtained after annealing a 1:1 mixture of $Mg(NH_2)_2$ and RbH. Indeed, except for some Bragg peaks from $Rb_2Mg(NH_2)_4$, the others are not attributable to any known Rb-containing amide, imide or nitride phases.

We also considered an alternative and more convenient synthesis route, described by reaction (2). According to the diffractogram in Fig. 1-b, the main reaction product is the same as from reaction (1).

2) $Rb_2Mg(NH_2)_4 + MgH_2 \rightarrow 2RbMgNH_2NH + 2H_2$

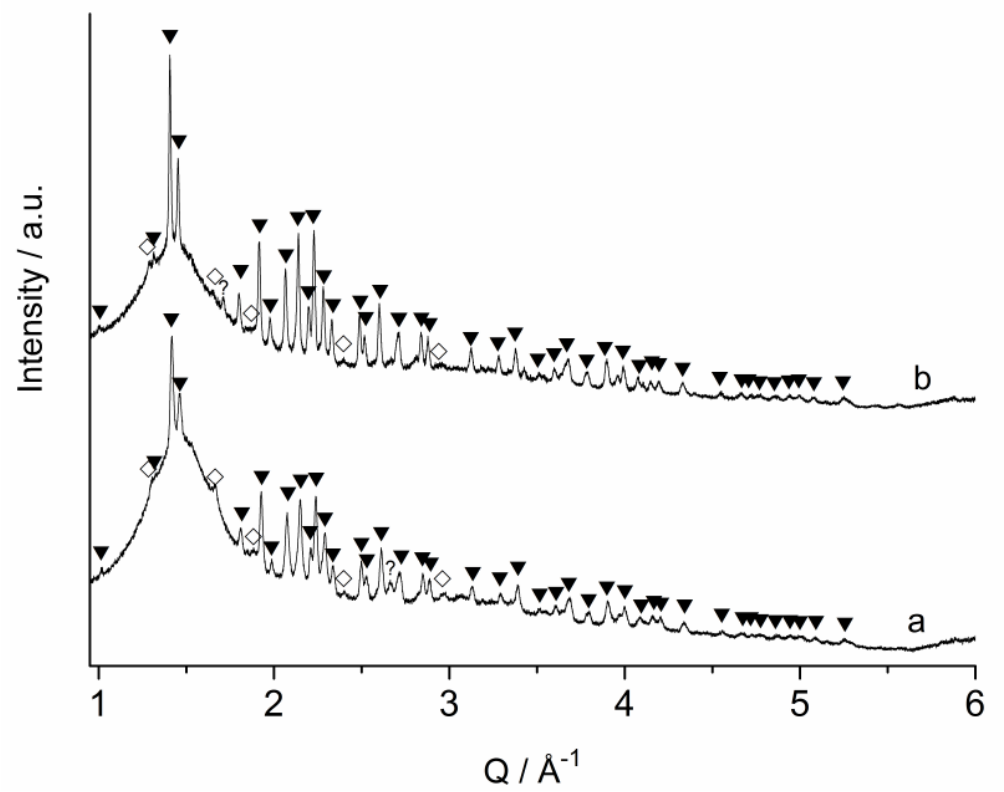


Figure 1. XPD patterns of the products obtained after annealing of $Mg(NH_2)_2$+RbH (a) and $Rb_2Mg(NH_2)_4$+$MgH_2$ (b). ▼ = New phase, ◇ = $Rb_2Mg(NH_2)_4$, ? = spurious peaks. λ = 1.54184 Å.

The deuterated compound $RbMgND_2ND$ was synthesized according to the second synthesis route, starting from $Rb_2Mg(ND_2)_4$ and $MgD_2$. Attenuated Total Reflection-Infrared spectroscopy (ATR-IR) was performed for further identification purpose (Fig. S1). For the $RbMgNH_2NH$ phase, the stretching signals of the N-H bonds are found at 3319 $cm^{-1}$ and 3261 $cm^{-1}$, very similar to the values of 3317 $cm^{-1}$ and 3260 $cm^{-1}$ reported from Li *et al.*,[20] and thus confirming the reproducibility of the synthesis. As predicted, the isotopic effect caused a red-shift of about 840 $cm^{-1}$ for the stretching signals of the N-D bonds in the deuterated compounds.

**Structure solution**

The formation of $RbMgNH_2NH$ was reported to be an important step for the reduced reaction enthalpy of Rb-doped Li-Mg-N-H systems.[20] Since increasing attention has been devoted to the study of similar systems, it is important to determine the structural model in order to provide a starting point for the development of plausible reaction mechanisms.

A SR-XPD pattern was collected at the SNBL at ESRF and used for structure determination. The high crystallinity of the sample, the high signal to noise ratio and the good resolution of the measurement, allowed the identification of the reflections belonging to the main phase, which were indexed in the orthorhombic crystal system with unit cell parameters: $a$ = 9.6282, $b$ = 3.7120 and $c$ = 10.1164 Å. From the systematic absences, the possible space group (s.g.) candidates were restricted to *Pnma* and $Pna2_1$. The structure was solved using FOX with the global optimization algorithm, excluding hydrogen atoms. For NPD data collected with the deuterated sample, the same procedure was used, but free deuterium atoms were included. For both space groups the global optimization provided very similar structure models, with the formula unit $RbMgN_2D_3$, in agreement with the stoichiometry predicted by Li *et al.*[20] The two space groups differ only in presence or absence of the inversion center. The differences in the Rietveld refinements were not significant, thus the highest symmetry space group *Pnma* was chosen. Finally, a combined Rietveld refinement of both NPD and XPD patterns was performed. The fits are presented in Fig. 2 and Fig. S2, respectively. Moreover, the structure model obtained after the combined refinement is presented in Fig. 3.

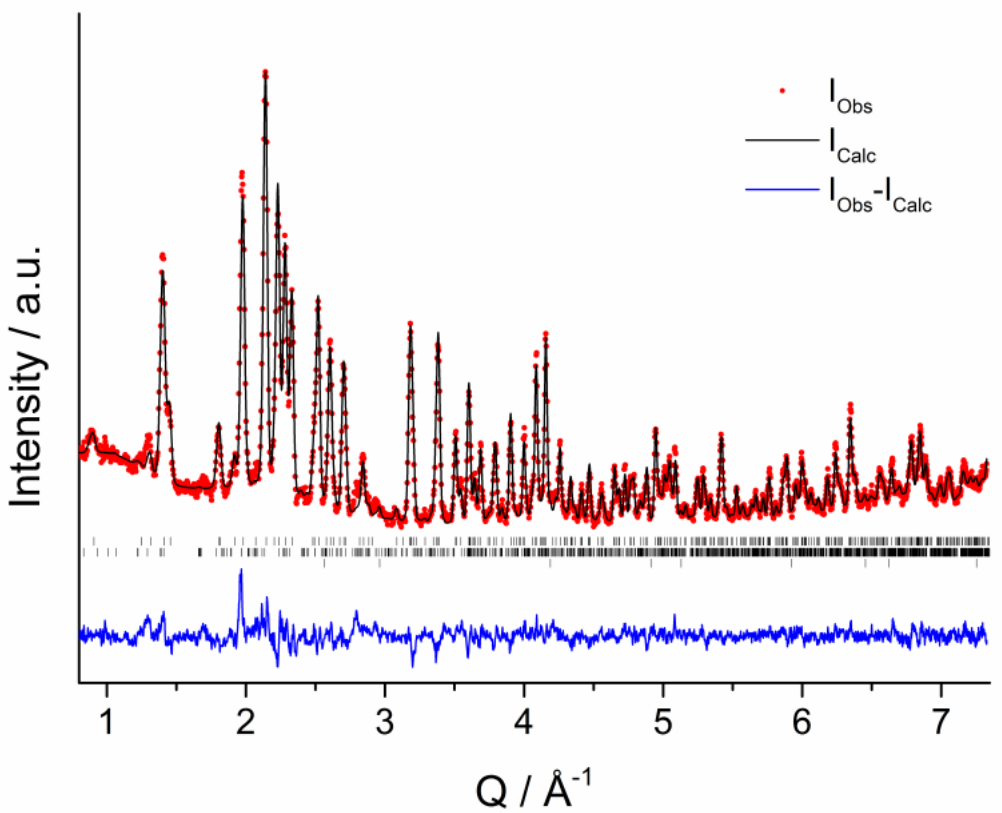


Figure 2. Rietveld refinement of the NPD pattern acquired at RT on the annealed $Rb_2Mg(ND_2)_4$+$MgD_2$ product. The figure shows the observed intensities (red dots), the calculated curve (black line), the Bragg reflections of the $RbMgND_2ND$ structure (vertical marks) and the difference plot (observed – calculated intensities, blue line). $R_{wp}$ = 0.0556 corrected for background; λ = 1.55357 Å.

Figure 3. Structure model of $RbMgND_2ND$ as obtained after Rietveld refinement with combined NPD and XPD data.

The unit cell contains 4 formula units, which gives a density of 2.67 g/cm$^3$, similar to that of α-$RbNH_2$ (2.64 g/cm$^3$)[33] and comparable to that of $Rb_2Mg(NH_2)_4$ (2.31 g/cm$^3$)[34]. Furthermore, $RbMgND_2ND$ is isostructural to $KMgND_2ND$.[35, 36] A comparison of the unit cell parameters of the two compounds is presented in Table 1 and the crystal structure parameters of $RbMgND_2ND$ are summarized in Table S1.

Table 1. Unit cell parameters and unit cell volume of the $RbMgND_2ND$ phase as obtained after Rietveld refinement of the NPD and XPD data. The values for $KMgND_2ND$ were taken from the work of Napolitano *et al.*[36] and are shown for comparison.

| | Experiment | *a* / Å | *b* / Å | *c* / Å | *V* / Å$^3$ |
|---|---|---|---|---|---|
| $KMgND_2ND$ | NPD | 9.3497(3) | 3.6631(1) | 9.8901(3) | 338.72(2) |

| | | | | | |
|---|---|---|---|---|---|
| $RbMgND_2ND$ | NPD+XPD | 9.55256(31) | 3.70772(11) | 10.08308(32) | 357.125(24) |

The unit cell volume is noticeably bigger in the case of $RbMgND_2ND$, which is reasonable considering the larger ionic radius of rubidium compared to potassium. From Table 2 it can be noticed that all but one of the $M^+$-N distances are longer in $RbMgND_2ND$ as compared to $KMgND_2ND$. Therefore, a bi-capped trigonal prism of amide and imide anions coordinating $Rb^+$, can be identified in this case (Fig. 4-a) as compared to the mono-capped trigonal prism reported for the $KMgND_2ND$.[36] A possible explanation for this difference is that, due to the longer radius, i.e. larger coordination sphere (see average $M^+$-N distance in Table 2), an additional amide group coordinates the $Rb^+$ in $RbMgND_2ND$. Conversely, the additional amide group is excluded from the first coordination sphere of $K^+$, because the shorter ionic radius is associated with a smaller coordination sphere and, therefore, shorter interatomic distances (stronger repulsions) between the amide and imide groups. Indeed, an average N-N distance of 4.7763(6) Å and 4.8781(7) Å can be calculated for the K- and Rb-phases, respectively. The nitrogen atoms considered for the calculation of the average N-N distance are displayed in Fig. 4-a and the values are reported in Table S2.

Table 2. Selected $M^+$-N distances ($d < 3.92$ Å) obtained from the structural models of $RbMgND_2ND$ (present work) and $KMgND_2ND$ (Napolitano *et al.*[36]). Longer distances in bold.

| Label | $d_1$, $d_2$ | $d_3$, $d_4$ | $d_5$ | $d_6$, $d_7$ | $d_8$ | Average |
|---|---|---|---|---|---|---|
| Multiplicity | 2 | 2 | 1 | 2 | 1 | - |
| $d_{K\text{-}N}$/Å | 3.071(6) | 3.378(6) | 3.097(7) | 2.937(6) | **3.910(7)** | 3.222(2) |
| $d_{Rb\text{-}N}$/Å | **3.269(3)** | **3.544(3)** | **3.255(4)** | **3.057(3)** | 3.523(4) | **3.3148(12)** |

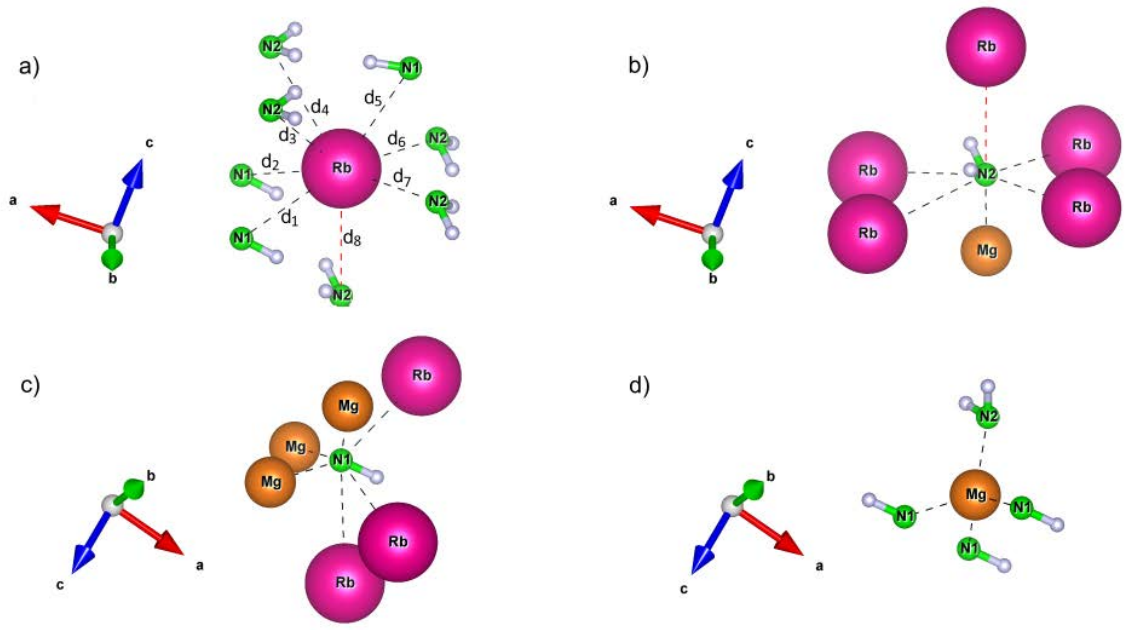


Figure 4. Structural coordination of a) $Rb^{+}$ (bi-capped trigonal prism), b) $NH_2^{-}$ (octahedron), c) $NH^{2-}$ (trigonal prism) and d) $Mg^{2+}$ (tetrahedron). All the geometries present considerable distortion as compared to the ideal case. The Rb-N distance of 3.523(4) Å is indicated by a dotted red line in a) and b).

The surrounding of the amide anion can be described considering the octahedral geometry proposed in Fig. 4-b. It is also possible to identify a triangular antiprism $Rb_3Mg_3$ around the imide anion (Fig. 4-c). This coordination entity is very similar in both the $KMgND_2ND$ and $RbMgND_2ND$ phases. Another interesting structural aspect that the two compounds have in common is the tetrahedral coordination of $Mg^{2+}$ to one $ND_2^{-}$ and three $ND^{2-}$ anions (Fig. 4-d). In fact, rather than displaying $[Mg(ND_2)(ND)_3]^{5-}$ isolated tetrahedrons, each imide anion coordinates to other three magnesium cations, building an infinite anionic chain in the [010] direction, counterbalanced by $Rb^{+}$ (Fig. 5).

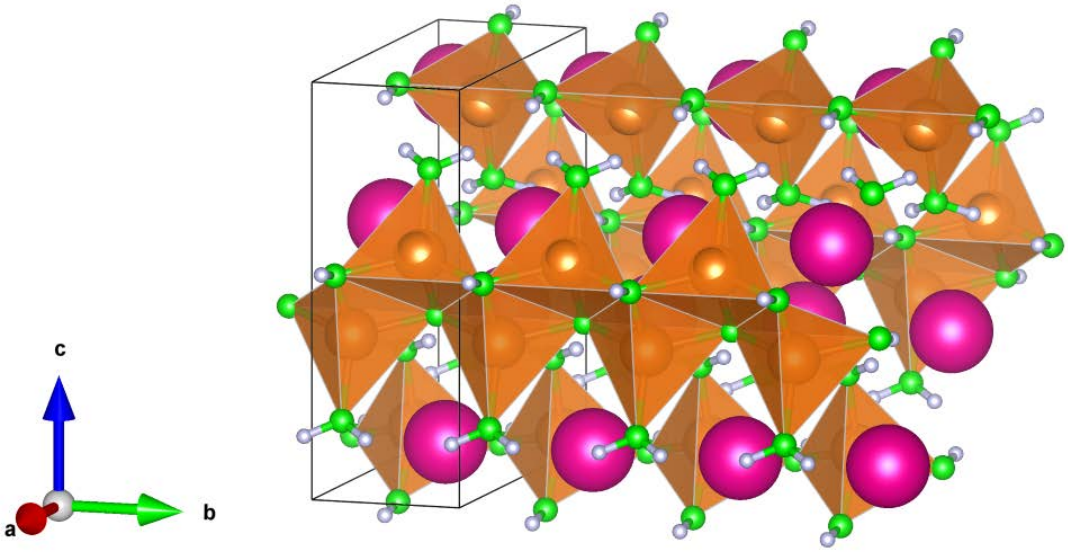


Figure 5. Infinite anionic chain of edge-sharing $[Mg(ND_2)(ND)_3]$ tetrahedrons in the [010] direction.

Similar features can be found in the structure of some double-cation tetrahydroborates ($Li_iA_j(BH_4)_{i+j}$; A = Rb, Cs).[37]

In this case, the amide anions completing the tetrahedral units are in terminal (i.e. non-bridging) positions because of an insufficient number of free electron pairs (Fig. 5). The deuterium atoms of the imide groups are equidistant (2.190(6) Å) from the closer deuterium atoms of each amide group in the adjacent chain and both amide and imide groups are oriented in order to minimize repulsions with the $Rb^+$ and $Mg^{2+}$ cations.

**Rb-N-H system**

Recently, new intermediate compositions were identified in the K-N-H system and reported as the first metal amide/hydride solid solution.[38] The same components were reported to take part in the desorption processes of K-Mg-N-H systems, promoting a novel amide-hydride anionic-

exchange mechanism.[39] Structural similarities between compounds of potassium and rubidium are not a peculiarity of bimetallic M-Mg-N-H systems, as they also occur in other classes of compounds, e.g. metal amides ($MNH_2$) and metal hydrides (MH). For this reason, here we present a systematic study of the $RbNH_2$-RbH system, in order to reveal the main similarities and differences with the $KNH_2$-KH case study.

Mixtures of $RbNH_2$ and RbH were prepared in different molar ratios (x = 0, 0.1, 0.3, 0.5, 0.7, 0.9, 1; with x indicating the molar fraction of $RbNH_2$), annealed and then characterized by *ex situ* XPD (Fig. 6).

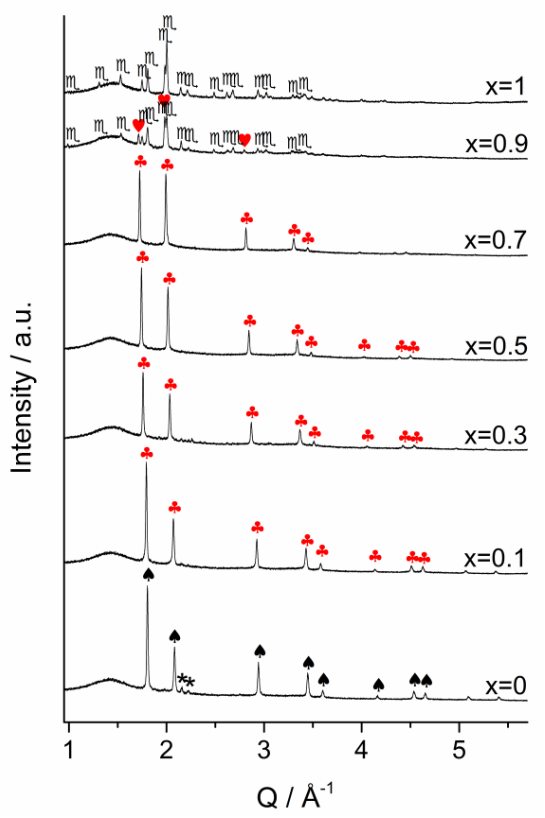


Figure 6. Diffractograms of the annealed $xRbNH_2+(1-x)RbH$ samples. ♠ = RbH ($Fm\bar{3}m$), ♣ = $Rb(NH_2)_xH_{(1-x)}$ ($Fm\bar{3}m$), ♥ = $RbNH_2$-like phase ($Fm\bar{3}m$), ♏ = $RbNH_2$ ($P2_1/m$), ✶ = RbOH ($P2_1/m$). λ = 1.54184 Å.

From the diffraction patterns collected after annealing, it is not possible to identify the Bragg reflections of the RT modification of $RbNH_2$ (monoclinic, s.g. $P2_1/m$) for the intermediate compositions 0.1, 0.3, 0.5 and 0.7. The diffractograms of these annealed samples are similar to the pattern of RbH (x = 0), except for a significant shift of the peak positions to lower Q-values and altered relative intensities. For x = 0.9 both the peaks of the monoclinic phase and the cubic phase can be identified.

To screen novel systems in general, sequential *in situ* XPD experiments with variable temperature can provide information on the composition, structure and reaction pathways of new

compounds.[40] In this case, in order to reveal how the starting components interacted during the annealing process, an *in situ* SR-XPD experiment was performed on a 1:1 molar mixture of $RbNH_2$ and RbH (Fig. 7).

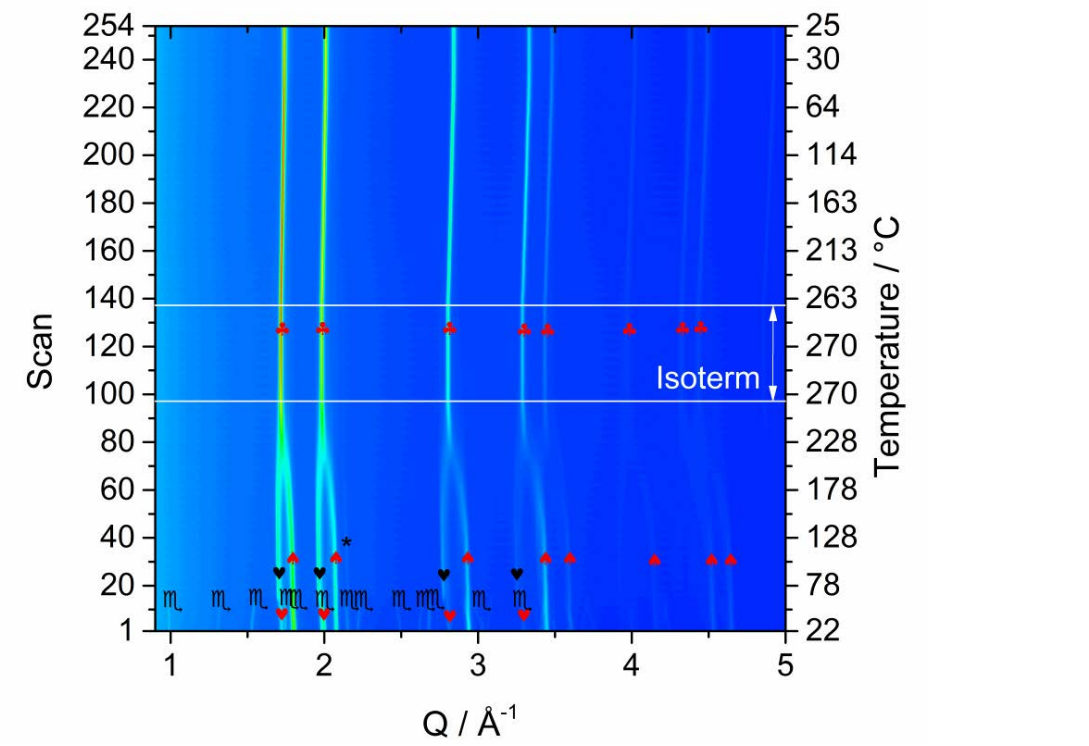


Figure 7. *In situ* XPD patterns acquired for the sample 0.5 $RbNH_2$ + 0.5 RbH. ♠ = RbH-like phase ($Fm\bar{3}m$), ♥ = $RbNH_2$-like phase ($Fm\bar{3}m$), ♏ = $RbNH_2$ ($P2_1/m$), ♥ = $RbNH_2$ ($Fm\bar{3}m$), ♣ = $Rb(NH_2)_xH_{(1-x)}$ ($Fm\bar{3}m$), ✶ = RbOH ($P2_1/m$). λ = 0.14235 Å.

In the diffraction pattern acquired at RT, the peaks of the monoclinic $RbNH_2$ are easy to identify (Fig. 7). Furthermore, the reflections of two cubic phases are also noticeable. The positions and relative intensities of the peaks of the two cubic phases, are similar to the values expected for RbH and the cubic polymorph of $RbNH_2$. When increasing the temperature, a phase transformation of

the monoclinic polymorph of $RbNH_2$ (monoclinic → cubic) occurs at ca. 65 °C. After the phase transformation, the peaks of these three cubic phases undergo a gradual shift and broadening, until they converge to a single set of sharp reflections. The evolution of the XPD data in Fig. 7 suggests that a continuous re-organization of the amide/hydride content takes place in each phase, until a single phase-composition is achieved at 270 °C. Indeed, all the three intermediate cubic phases, as well as the final single phase product, can be successfully fitted taking into account $NH_2^-/H^-$ substitution and cell expansion in the structural model of RbH (Fig. S3). The final cubic phase formed at 270 °C is retained during the entire cooling process to RT (Fig. 7).

The *in situ* experiments were performed for all the examined compositions (Fig. S4-S9). In every case the formation of a single phase composition is achieved at 270 °C. The values of the unit cell parameters, as obtained by Rietveld refinements of the diffractograms acquired during isothermal conditions (T = 270 °C), are plotted against the composition, confirming that the amide/hydride substitution causes expansion of the unit cell over the whole compositional range (Fig. S10).

For the composition x=0.9, the formation of a single cubic phase is achieved at T = 270 °C, but after cooling some new peaks appeared at RT (Fig. S8). Unfortunately, it is not possible to fit the peaks with the monoclinic model of $RbNH_2$ or to attempt a structure solution, due to the low intensity and small number of Bragg reflections available. Nonetheless, it can be noticed that the formation of the new peaks is associated with a decrease in the intensity of the peaks of the cubic phase (Fig. S8). The changes in the XPD patterns suggest that a slow segregation process started to take place, involving an intermediate structure. This structure, after some time, may be transformed into the monoclinic phase of $RbNH_2$, as it was revealed in the *ex situ* experiments at RT (Fig. 6). Therefore, at RT, full solubility into the cubic phase seems to be achievable, except when the content of amide phase (monoclinic at RT) is too high ($x \geq 0.9$).

A solid-state NMR (SSNMR) investigation on the composition x = 0.5 annealed and hand-ground samples was carried out to independently assess the formation of solid solutions rather than heterogeneous mixtures. In the $^{1}$H MAS spectra (Fig. 8), no significant shifts were observed on passing from the starting materials to the annealed and ground samples (Table 3).

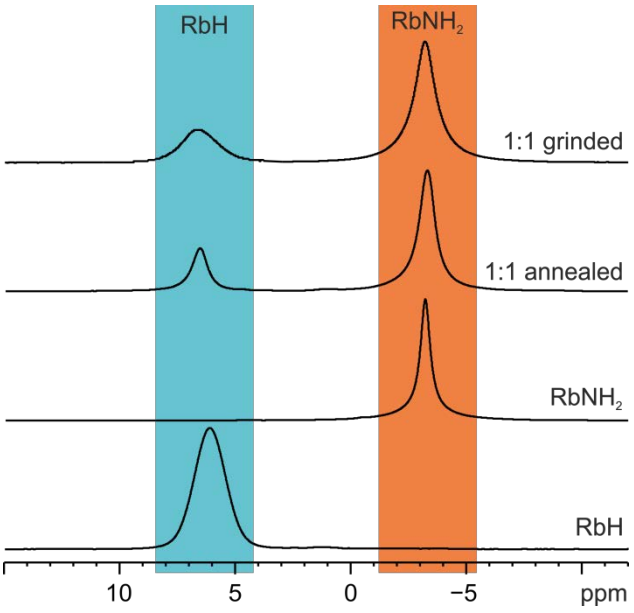


Figure 8. a) $^{1}$H (400.23 MHz) MAS SSNMR spectra of starting reagents, 0.5$RbNH_2$+0.5RbH annealed and 0.5$RbNH_2$+0.5RbH ground recorded with a spinning speed of 32 kHz.

Table 3. $^{1}$H chemical shifts (ppm) with assignments and $T_1$ $^{1}$H (s) values for the samples RbH, $RbNH_2$, 0.5$RbNH_2$+0.5RbH annealed and 0.5$RbNH_2$+0.5RbH ground.

| | RbH peak | | $RbNH_2$ peak | |
|---|---|---|---|---|
| Sample | δ | $T_1$ $^{1}$H | δ | $T_1$ $^{1}$H |
| RbH | 6.1 | 7.8 | - | - |
| $RbNH_2$ | - | - | −3.2 | 30.6 |

| | | | | |
|---|---|---|---|---|
| Annealed | 6.5 | 4.9 | −3.3 | 4.4 |
| Ground | 6.6 | 7.4 | −3.2 | 26.4 |

$T_1$ $^1$H relaxation measurements (Table 3) on the annealed sample show almost the same value for the RbH and $RbNH_2$ resonances (4.9 and 4.4 s, respectively) compared to those of the starting compounds (7.8 and 30.6 s, respectively). This is only possible when a spin diffusion process is active, i.e. if the protons belong to the same phase or in the case of homogeneous samples on a nanometer scale.[41]

Direct evidence of the solid solution formation is provided by the $^1$H double-quantum (DQ) MAS SSNMR experiment (Fig. 9). Certainly, the observed DQ correlation ($\delta_{DQ}$ = 3.2) between the RbH (6.5 ppm) and $RbNH_2$ (−3.3 ppm) signals implies that they are in close spatial proximity to each other (less than 5 Å).[42] This is possible only if they are intimately related, as in a solid solution.[43]

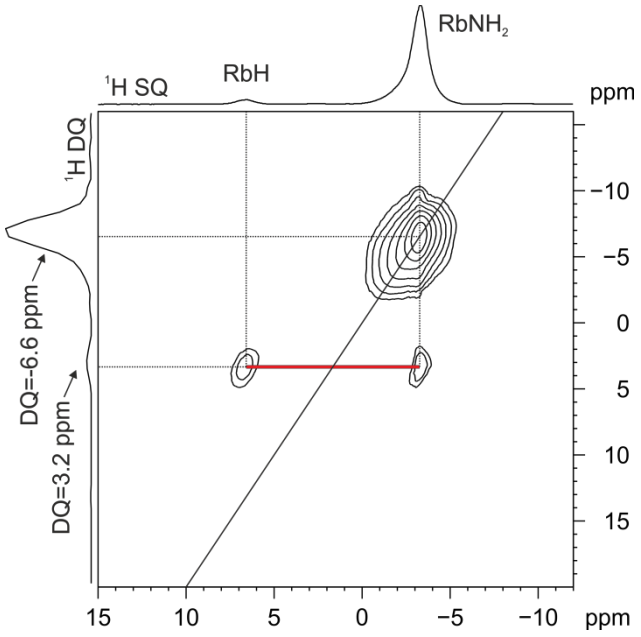


Figure 9. 2D $^{1}$H (400.23 MHz) DQ MAS SSNMR spectrum of the 0.5$RbNH_2$+0.5RbH sample after annealing, recorded with a spinning speed of 32 kHz. The red line highlights the DQ correlation between the RbH and $RbNH_2$ signals.

Similar correlation is also observed for the ground sample (ESI, Fig. S11), which can be explained with the formation of a solid solution already without annealing. Interestingly, the degree of mixing of RbH and $RbNH_2$ in this case seems to be much lower: in fact, an auto-peak ($\delta_{DQ}$ = 13.2) in the $^{1}$H DQ MAS spectrum, highlighting proximity between RbH protons. This signal, not present in the annealed sample, indicates that the RbH unit cells are organized in clusters and are mixed with clusters of $RbNH_2$ unit cells. This is supported in the $T_1$ $^{1}$H relaxation measurements (Table 3), which show different $T_1$ values for the RbH and $RbNH_2$ resonances (7.4 and 26.4 s, respectively) indicating the presence of distinct RbH and $RbNH_2$ domains much larger than 100 Å.

**Structural analogies**

The present work highlights two new cases of structural analogies between potassium and rubidium amide based systems: the $MNH_2$-MH solid solution and the $MMgNH_2NH$ phase (M = K, Rb).

Metal hydrides of alkaline metals are known to crystallize in the cubic crystal system with symmetry $Fm\bar{3}m$. Instead, metal amides offer a higher variety of crystal structures. In particular for both $KNH_2$ and $RbNH_2$ a low temperature and a high temperature polymorph are known, the first one is monoclinic (s.g. $P2_1/m$)[33, 44], the second one cubic (s.g. $Fm\bar{3}m$).[45] However, in the case of potassium amide an additional polymorph (tetragonal, s.g. $P4/nmm$) was reported as intermediate structure between the high and low temperature modifications, while for $RbNH_2$ this structural modification was not observed, in agreement with our *in situ* SR-XPD experiments.[46] Moreover, for $KNH_2$ the transformation to cubic symmetry takes place at about 75 °C,[46] while in the case of $RbNH_2$ it occurs already at 65 °C (present work) or even at lower temperatures (40-45 °C in the pioneering studies).[47] For $CsNH_2$, the low temperature modification is tetragonal (s.g. $P4/nmm$) rather than monoclinic and the polymorphic change to cubic (s.g. $Pm\bar{3}m$) occurs already at 30-35 °C.[47] Therefore, the lower limit of the stability range of the cubic phase is progressively shifted to lower temperatures in the order: K, Rb, Cs. The size of the cation seems to affect also the solubility at RT. For the $KNH_2$-KH system full solubility was achieved at RT only when the content of the amide phase was very low (x = 0.1).[38] In this case it is possible to achieve full solubility for all the compositions, except for x = 0.9 (Fig. 6).

The cation seems to have an effect also on the reactivity of the system. In the $KNH_2$-KH system the peaks of the solid solution were not present or barely detectable after hand grinding, and the sample consisted essentially of unreacted $KNH_2$ and KH.[38] However, in the diffractograms of the $RbNH_2$-RbH system (Fig. 7 and Fig. S5-S9) strong peaks belonging to the intermediate

compositions are present already after hand grinding for all the mixed samples (x = 0.1, 0.3, 0.5, 0.7, 0.9). These results suggest that the larger cation hastens the kinetics of the dissolution process at RT.

The structural properties of the $RbMgNH_2NH$ phase, as experimentally determined in the present work, fit very well in the crystal chemistry of metal amides. Among the known alkali and alkaline-earth metal amides with the formula $M_2Mg(NH_2)_4$ (M = K, Rb, Cs), isotypic phases are formed only for M = K, Rb.[34, 48] With the present work, the isostructural relationship of $MMgNH_2NH$ phases is also demonstrated for M = K, Rb. The main differences are the increased unit cell volume and the coordination number of the monovalent cation; they are both a consequence of the different ionic radius of $M^+$. Considering that the formation of a $CsMgNH_2NH$ phase was recently suggested,[18, 49] it will be interesting to compare its crystal structure to the one of $KMgNH_2NH$ and $RbMgNH_2NH$ to determine whether or not an isotypic compound is formed or any common structural features can be identified. $KMgNH_2NH$ and $RbMgNH_2NH$ represent, to the best of our knowledge, the first example of double cation ordered amide-imide.

Taking into account the isostructurality of $KMgNH_2NH$/$RbMgNH_2NH$ and the effects that Rb-based additives have on the hydrogen storage properties of Li-Mg-N-H systems, it is interesting to recall the possible mechanisms previously proposed for the $KMgNH_2NH$ phase.[36] Both structures show more dense packing along the [100] and [001] directions (ESI, Fig. S12), while along the [010] direction the presence of voids and channels could promote the diffusion of hydrogen, thus mitigating the negative impact of sintering and particle growth. Moreover, the *b*-axis of the orthorhombic unit cell is significantly smaller than the other two axes, and also smaller than the interatomic distances between atoms of the same type within the unit cell. Thus, if we consider the same type of atoms, the longest atomic chain with the shortest interatomic distances runs along the

*b*-axis. For this reason the [010] direction would probably be the most favorite pathway for diffusion of ionic species by vacancies.

A progressive loss of reversibility due to coarsening of the particles was reported for some K-based additives, while good reversibility over 30-50 cycles was obtained when Rb- or Cs-based additives were employed in combination with K.[15, 18, 21] A critical consideration of these results suggests that, in some cases, microstructural effects might be overwhelming as compared to the mechanisms that can be drawn on an atomistic scale. Nevertheless, the fact that the formation of stable $MMgNH_2NH$ phases (M = K, Rb, Cs) can improve the sorption properties of Li-Mg-N-H systems, indicates a possible direction for the successful design of improved additives.

## CONCLUSIONS

$RbMgNH_2NH$ was found to be isostructural to $KMgNH_2NH$. The analogies (atomic composition and space group) and differences (interatomic distances, density and surrounding of $M^+$) found for the two compounds are in good agreement with the general picture provided by the crystal chemistry of metal amides. The Rb-N-H system represents a further example of the structural analogies between amides of potassium and rubidium. The formation of an amide-hydride solid solution takes place, similarly to the K-N-H system. However, for rubidium it is possible to reach solubility for a much larger compositional range even at room temperature, indicating a stronger driving force towards the dissolution process. The main reason for these differences, most probably, relies on the stabilization effect that $Rb^+$ has over the cubic polymorph, which is reflected in the lowered temperatures of the phase transformations, as well. Additionally, the formation of appreciable amounts of solid solution after hand grinding indicates that $Rb^+$ improves the kinetics of the dissolution process at RT.

To the best of our knowledge K and Rb are the unique alkali metals able to form a mixed amide-imide phase with Mg as well as amide-hydride solid solutions. The co-existence of amide-imide and amide-hydride anions, in the same crystal might be one of the reasons why K and Rb based additives are so effective in improving the hydrogen storage properties of Li-Mg-N-H systems.

## ASSOCIATED CONTENT

Structural details of $RbMgND_2ND$, graphics of the ATR-IR measurements, additional Rietveld refinements, *in situ* SR-XPD experiments, cell parameters and $^1H$ double-quantum (DQ) MAS SSNMR. This material is available free of charge via the Internet at http://pubs.acs.org.

## Author Contributions

The manuscript was written through contributions of all authors. All authors have given approval to the final version of the manuscript.

## ACKNOWLEDGMENT

The research leading to these results has received funding from the European Marie Curie Actions under ECOSTORE grant agreement no. 607040. The authors acknowledge the Swiss-Norwegian Beamlines of ESRF and Norbert Schell (DESY) for the allocation of beamtime and excellent support with the data collection. The authors also thank CONICET (Consejo Nacional de Investigaciones Científicas y Técnicas), ANPCyT – (Agencia Nacional de Promoción Científica y Tecnológica), CNEA (Comisión Nacional de Energía Atómica).

Insert Table of Contents Graphic and Synopsis Here


1. Davy, H. The Bakerian Lecture: An Account of Some New Analytical Researches on the Nature of Certain Bodies, Particularly the Alkalies, Phosphorus, Sulphur, Carbonaceous Matter, and the Acids Hitherto Undecompounded; With Some General Observations on Chemical Theory. *Philosophical Transactions of the Royal Society of London* **1809,** 99, 39-104 DOI: doi:10.1098/rstl.1809.0005.
2. Gay-Lussac, J. L.; Thénard, L. J. Notiz über das Kali - und das Natron - Metall. *Annalen der Physik* **1809,** 32 (5), 23-39.
3. Gay-Lussac, J. L.; Thénard, L. J. Sur la Préparation chimique et les Propriétés du Potassium et

du Sodium. *Recherches physico-chimiques* **1811,** 1, 337-356.
4. Dafert, F. W.; Miklauz, R. Über einige neue Verbindungen von Stickstoff und Wasserstoff mit Lithium. *Monatshefte für Chemie* **1910,** 31 (9), 981-996 DOI: 10.1007/BF01518423.
5. Chen, P.; Xiong, Z.; Luo, J.; Lin, J.; Tan, K. L. Interaction of hydrogen with metal nitrides and imides. *Nature* **2002,** 420 (6913), 302-304 DOI: http://www.nature.com/nature/journal/v420/n6913/suppinfo/nature01210_S1.html.
6. Cao, H.; Zhang, Y.; Wang, J.; Xiong, Z.; Wu, G.; Chen, P. Materials design and modification on amide-based composites for hydrogen storage. *Progress in Natural Science: Materials International* **2012,** 22 (6), 550-560 DOI: http://dx.doi.org/10.1016/j.pnsc.2012.11.013.
7. Xiong, Z.; Hu, J.; Wu, G.; Chen, P.; Luo, W.; Gross, K.; Wang, J. Thermodynamic and kinetic investigations of the hydrogen storage in the Li–Mg–N–H system. *Journal of Alloys and Compounds* **2005,** 398 (1), 235-239 DOI: http://dx.doi.org/10.1016/j.jallcom.2005.02.010.
8. Wang, J.; Liu, T.; Wu, G.; Li, W.; Liu, Y.; Araújo, C. M.; Scheicher, R. H.; Blomqvist, A.; Ahuja, R.; Xiong, Z.; Yang, P.; Gao, M.; Pan, H.; Chen, P. Potassium-Modified Mg(NH2)2/2 LiH System for Hydrogen Storage. *Angewandte Chemie International Edition* **2009,** 48 (32), 5828-5832 DOI: 10.1002/anie.200805264.
9. Durojaiye, T.; Goudy, A. Desorption kinetics of lithium amide/magnesium hydride systems at constant pressure thermodynamic driving forces. *International Journal of Hydrogen Energy* **2012,** 37 (4), 3298-3304 DOI: http://dx.doi.org/10.1016/j.ijhydene.2011.11.071.
10. Luo, W.; Stavila, V.; Klebanoff, L. E. New insights into the mechanism of activation and hydrogen absorption of (2LiNH2–MgH2). *International Journal of Hydrogen Energy* **2012,** 37 (8), 6646-6652 DOI: http://dx.doi.org/10.1016/j.ijhydene.2012.01.019.
11. Liang, C.; Liu, Y.; Gao, M.; Pan, H. Understanding the role of K in the significantly improved hydrogen storage properties of a KOH-doped Li-Mg-N-H system. *Journal of Materials Chemistry A* **2013,** 1 (16), 5031-5036 DOI: 10.1039/C3TA01071F.

12. Liu, Y.; Li, C.; Li, B.; Gao, M.; Pan, H. Metathesis Reaction-Induced Significant Improvement in Hydrogen Storage Properties of the KF-Added Mg(NH2)2–2LiH System. *The Journal of Physical Chemistry C* **2013,** 117 (2), 866-875 DOI: 10.1021/jp3107414.
13. Wang, J.; Chen, P.; Pan, H.; Xiong, Z.; Gao, M.; Wu, G.; Liang, C.; Li, C.; Li, B.; Wang, J. Solid–Solid Heterogeneous Catalysis: The Role of Potassium in Promoting the Dehydrogenation of the Mg(NH2)2/2 LiH Composite. *ChemSusChem* **2013,** 6 (11), 2181-2189 DOI: 10.1002/cssc.201200885.
14. Li, C.; Liu, Y.; Pang, Y.; Gu, Y.; Gao, M.; Pan, H. Compositional effects on the hydrogen storage properties of Mg(NH2)2-2LiH-xKH and the activity of KH during dehydrogenation reactions. *Dalton transactions* **2014,** 43 (6), 2369-2377 DOI: 10.1039/C3DT52296B.
15. Li, C.; Liu, Y.; Yang, Y.; Gao, M.; Pan, H. High-temperature failure behaviour and mechanism of K-based additives in Li-Mg-N-H hydrogen storage systems. *Journal of Materials Chemistry A* **2014,** 2 (20), 7345-7353 DOI: 10.1039/C4TA00025K.
16. Liu, Y.; Yang, Y.; Zhang, X.; Li, Y.; Gao, M.; Pan, H. Insights into the dehydrogenation reaction process of a K-containing Mg(NH2)2-2LiH system. *Dalton transactions* **2015,** 44 (41), 18012-18018 DOI: 10.1039/C5DT03334A.
17. Lin, H.-J.; Li, H.-W.; Paik, B.; Wang, J.; Akiba, E. Improvement of hydrogen storage property of three-component Mg(NH2)2-LiNH2-LiH composites by additives. *Dalton transactions* **2016,** 45 (39), 15374-15381 DOI: 10.1039/C6DT02845D.
18. Zhang, J.; Wang, Y.; Zhang, M.; Leng, Z.; Gao, M.; Hu, J.; Liu, Y.; Pan, H. Improved overall hydrogen storage properties of a CsH and KH co-doped Mg(NH2)2/2LiH system by forming mixed amides of Li-K and Cs-Mg. *RSC Advances* **2017,** 7 (48), 30357-30364 DOI: 10.1039/C7RA05166B.
19. Durojaiye, T.; Hayes, J.; Goudy, A. Rubidium Hydride: An Exceptional Dehydrogenation Catalyst for the Lithium Amide/Magnesium Hydride System. *The Journal of Physical Chemistry C* **2013,** 117 (13), 6554-6560 DOI: 10.1021/jp400961k.
20. Li, C.; Liu, Y.; Gu, Y.; Gao, M.; Pan, H. Improved Hydrogen-Storage Thermodynamics and Kinetics for an RbF-Doped Mg(NH2)2–2 LiH System. *Chemistry – An Asian Journal* **2013,** 8 (9), 2136-2143 DOI: 10.1002/asia.201300323.
21. Li, C.; Liu, Y.; Ma, R.; Zhang, X.; Li, Y.; Gao, M.; Pan, H. Superior Dehydrogenation/Hydrogenation Kinetics and Long-Term Cycling Performance of K and Rb Cocatalyzed Mg(NH2)2-2LiH system. *ACS Applied Materials & Interfaces* **2014,** 6 (19), 17024-17033 DOI: 10.1021/am504592x.
22. Durojaiye, T.; Hayes, J.; Goudy, A. Potassium, rubidium and cesium hydrides as dehydrogenation catalysts for the lithium amide/magnesium hydride system. *International Journal of Hydrogen Energy* **2015,** 40 (5), 2266-2273 DOI: http://dx.doi.org/10.1016/j.ijhydene.2014.12.056.
23. Hayes, J.; Durojaiye, T.; Goudy, A. Hydriding and dehydriding kinetics of RbH-doped 2LiNH2/MgH2 hydrogen storage system. *Journal of Alloys and Compounds* **2015,** 645, Supplement 1, S496-S499 DOI: https://doi.org/10.1016/j.jallcom.2014.12.074.
24. Dyadkin, V.; Pattison, P.; Dmitriev, V.; Chernyshov, D. A new multipurpose diffractometer PILATUS@SNBL. *Journal of Synchrotron Radiation* **2016,** 23 (3), 825-829 DOI: 10.1107/S1600577516002411.

25. Hauback, B. C.; Fjellvåg, H.; Steinsvoll, O.; Johansson, K.; Buset, O. T.; Jørgensen, J. The High Resolution Powder Neutron Diffractometer PUS at the JEEP II Reactor at Kjeller in Norway. *Journal of Neutron Research* **2000,** 8 (3), 215-232 DOI: 10.1080/10238160008200055.
26. Favre-Nicolin, V.; Cerny, R. FOX, `free objects for crystallography': a modular approach to ab initio structure determination from powder diffraction. *Journal of Applied Crystallography* **2002,** 35 (6), 734-743 DOI: doi:10.1107/S0021889802015236.
27. Rietveld, H. M., Line profiles of neutron powder-diffraction peaks for structure refinement Acta Crystallographica Volume 22, Issue 1. In *Acta Crystallographica*, 1967; Vol. 22, pp 151-152.
28. Rietveld, H. M., A profile refinement method for nuclear and magnetic structures Journal of Applied Crystallography Volume 2, Issue 2. In *Journal of Applied Crystallography*, 1969; Vol. 2, pp 65-71.
29. Lutterotti, L.; Matthies, S.; Wenk, H. R.; Schultz, A. S.; Richardson, J. W. Combined texture and structure analysis of deformed limestone from time-of-flight neutron diffraction spectra. *J Appl Phys* **1997,** 81 (2), 594-600.
30. Dreele, A. C. L. a. R. B. V. General Structure Analysis System (GSAS). *Los Alamos National Laboratory Report LAUR 86-748* **2000**.
31. Toby, B. EXPGUI, a graphical user interface for GSAS. *Journal of Applied Crystallography* **2001,** 34 (2), 210-213 DOI: doi:10.1107/S0021889801002242.
32. Momma, K.; Izumi, F. VESTA 3 for three-dimensional visualization of crystal, volumetric and morphology data. *Journal of Applied Crystallography* **2011,** 44 (6), 1272-1276 DOI: doi:10.1107/S0021889811038970.
33. Juza, R.; Jacobs, H.; Klose, W. Die Kristallstrukturen der Tieftemperaturmodifikationen von RbNH2 und KNH2. *Naturwissenschaften* **1962,** 49 (2), 35-36 DOI: 10.1007/BF00596466.
34. Jacobs, H.; Birkenbeul, J.; Kockelkorn, J. Darstellung und eigenschaften der amidomagnesate des kaliums und rubidiums K2[Mg(NH2)4]- und Rb2[Mg(NH2)4]-Verbindungen mit isolierten [Mg(NH2)4]2−-tetraedern. *Journal of the Less Common Metals* **1984,** 97, 205-214 DOI: http://dx.doi.org/10.1016/0022-5088(84)90024-9.
35. Wang, J. H.; Wu, G. T.; Chua, Y. S.; Guo, J. P.; Xiong, Z. T.; Zhang, Y.; Gao, M. X.; Pan, H. G.; Chen, P. Hydrogen Sorption from the Mg(NH2)(2)-KH System and Synthesis of an Amide-Imide Complex of KMg(NH)(NH2). *ChemSusChem* **2011,** 4 (11), 1622-1628.
36. Napolitano, E.; Dolci, F.; Campesi, R.; Pistidda, C.; Hoelzel, M.; Moretto, P.; Enzo, S. Crystal structure solution of KMg(ND)(ND2): An ordered mixed amide/imide compound. *International Journal of Hydrogen Energy* **2014,** 39 (2), 868-876 DOI: http://dx.doi.org/10.1016/j.ijhydene.2013.10.131.
37. Schouwink, P.; Smrcok, L.; Cerny, R. Role of the Li+ node in the Li-BH4 substructure of double-cation tetrahydroborates. *Acta Crystallographica Section B* **2014,** 70 (5), 871-878 DOI: 10.1107/S2052520614017351.
38. Santoru, A.; Pistidda, C.; Sorby, M. H.; Chierotti, M. R.; Garroni, S.; Pinatel, E.; Karimi, F.; Cao, H.; Bergemann, N.; Le, T. T.; Puszkiel, J.; Gobetto, R.; Baricco, M.; Hauback, B. C.; Klassen, T.; Dornheim, M. KNH2-KH: a metal amide-hydride solid solution. *Chemical communications* **2016,** 52 (79), 11760-11763 DOI: 10.1039/C6CC05777B.
39. Santoru, A.; Garroni, S.; Pistidda, C.; Milanese, C.; Girella, A.; Marini, A.; Masolo, E.; Valentoni, A.; Bergemann, N.; Le, T. T.; Cao, H.; Haase, D.; Balmes, O.; Taube, K.; Mulas, G.; Enzo, S.; Klassen, T.; Dornheim, M. A new potassium-based intermediate and its role in the

desorption properties of the K-Mg-N-H system. *Physical Chemistry Chemical Physics* **2016,** 18 (5), 3910-3920 DOI: 10.1039/C5CP06963G.
40. Ravnsbæk, D. B.; Sørensen, L. H.; Filinchuk, Y.; Besenbacher, F.; Jensen, T. R. Screening of Metal Borohydrides by Mechanochemistry and Diffraction. *Angewandte Chemie International Edition* **2012,** 51 (15), 3582-3586 DOI: 10.1002/anie.201106661.
41. Gaglioti, K.; Chierotti, M. R.; Grifasi, F.; Gobetto, R.; Griesser, U. J.; Hasa, D.; Voinovich, D. Improvement of the water solubility of tolfenamic acid by new multiple-component crystals produced by mechanochemical methods. *CrystEngComm* **2014,** 16 (35), 8252-8262 DOI: 10.1039/C4CE00549J.
42. Chierotti, M. R.; Gobetto, R. NMR crystallography: the use of dipolar interactions in polymorph and co-crystal investigation. *CrystEngComm* **2013,** 15 (43), 8599-8612 DOI: 10.1039/C3CE41026A.
43. Braga, D.; Chelazzi, L.; Grepioni, F.; Dichiarante, E.; Chierotti, M. R.; Gobetto, R. Molecular Salts of Anesthetic Lidocaine with Dicarboxylic Acids: Solid-State Properties and a Combined Structural and Spectroscopic Study. *Crystal Growth & Design* **2013,** 13 (6), 2564-2572 DOI: 10.1021/cg400331h.
44. Juza, R.; Jacobs, H.; Klose, W. Die Kristallstrukturen der Tieftemperaturmodifikationen von Kalium- und Rubidiumamid. *Zeitschrift für anorganische und allgemeine Chemie* **1965,** 338 (3-4), 171-178 DOI: 10.1002/zaac.19653380309.
45. Juza, R.; Liedtke, H. Zur Kenntnis des Kaliumamids. *Zeitschrift für anorganische und allgemeine Chemie* **1957,** 290 (3-4), 205-208 DOI: 10.1002/zaac.19572900310.
46. Jacobs, H.; Von Osten, E., Notizen: Die Kristallstruktur einer neuen Modifikation des Kaliumamids, KNH2. In *Zeitschrift für Naturforschung B*, 1976; Vol. 31, p 385.
47. Juza, R.; Mehne, A. Zur Kristallstruktur der Alkalimetallamide. *Zeitschrift für anorganische und allgemeine Chemie* **1959,** 299 (1-2), 33-40 DOI: 10.1002/zaac.19592990105.
48. Jacobs, H.; Birkenbeul, J.; Schmitz, D. Strukturverwandtschaft des dicaesiumamidomagnesats, Cs2[Mg(NH2)4], zum β-K2SO4-Typ. *Journal of the Less Common Metals* **1982,** 85, 79-86 DOI: http://dx.doi.org/10.1016/0022-5088(82)90060-1.
49. Zhang, J.; Liu, Y.; Zhang, X.; Yang, Y.; Zhang, Q.; Jin, T.; Wang, Y.; Gao, M.; Sun, L.; Pan, H. Synthesis of CsH and its effect on the hydrogen storage properties of the Mg(NH2)2-2LiH system. *International Journal of Hydrogen Energy* **2016,** 41 (26), 11264-11274 DOI: http://dx.doi.org/10.1016/j.ijhydene.2016.04.057.